# Selected Physico-Chemical Properties of Composite Scaffolds of Sintered Submicrocrystalline Corundum and Bioglass

**Barbara Staniewicz-Brudnik**
Krakow Institute of Technology
**Malgorzata Karolus** ( karolus@us.edu.pl )
Institute of Material Science, University of Silesia https://orcid.org/0000-0002-2388-8036
**Katarzyna Cholewa-Kowalska**
AGH University of Science and Technology
**Grzegorz Skrabalak**
Krakow Institute of Technology
**Jolanta Laszkiewicz-Łukasik**
Krakow Institute of Technology
**Justyna Drukała**
Jagiellonian University
**Joanna Stalińska**
Jagiellonian University
**Katarzyna Dziedzic**
Jagiellonian University

**Research Article**

**Keywords:** submicrocrystalline sintered corundum, bioglass, scaffolds, SEM, XRD, SBF, surface topography

**Posted Date:** September 2nd, 2021

**DOI:** https://doi.org/10.21203/rs.3.rs-849049/v1



**Version of Record:** A version of this preprint was published at The International Journal of Advanced Manufacturing Technology on February 16th, 2022. See the published version at https://doi.org/10.1007/s00170-022-08736-w.

# Abstract

Presented paper contains description and interpretation of the results of selected physicochemical and structural properties of two types of composite sinters. They were constituted of a mixture of sintered microcrystalline corundum and bioglass $CaO$-$P_2O_5$-$SiO_2$-$Na_2O$ system intended for scaffolds to cell culture of human chondrocytes. The composites contained a mixture of both above-mentioned components in the volumetric proportion of 50:50 (W5) and 30:70 (W7). They were obtained using powder metallurgy by free sintering in air atmosphere. Phase analysis of composites and verification of theoretical identification using X-ray diffraction were performed. The same phases were found in both cases ($Al_2O_3$ $SiO_2$ $CaAl_2Si_2O_8$, $Ca_3$ $(PO_4)_2$, $Ca_2Al_4O_7$ and $NaAlSiO_4$. Microscopic tests of composite surfaces were performed and some differences were found. W5 sample was not completely covered with bioglass, whilst W7 sample was completely covered with bioglass with few fine pores. Tests of surface topography confirmed the presence of large and small pores. Composite surfaces immersed for 30 days in artificial blood plasma were tested and then electron microscopy analysis was performed. It was found that no significant changes occurred on the surface of the W5 composite, probably partial corrosion of the glass happened. Spherical forms characteristic of HA-hydroxyapatites were observed on the surface of sample W7. Human chondrocyte cells were seeded on both types of sinters and proliferation assay was performed on them with positive results.


# Highligts

scaffolds composites, structure identification by VCS algorythm and XRD diffraction, surface topography of scaffolds, SBF test, proliferation test of chondrocite

# Introduction

The dynamic development of biomaterial engineering, the search for new biocompatible substances and materials that can replace damaged tissues and organs have caused a change in the proportion of biomaterials (metals and metal alloys, polymers and inorganic composites) towards composite materials over the past two decades. The demand for biomaterials results mostly from the growing number of communication injuries, injuries resulting from practicing sports, including extreme sports, and development of civilization diseases. It is also associated with progress in the development of various fields of reconstructive surgery, interventional surgery and prosthetics[1,2,3,4]. One of the most interesting biocomposites used in bone regenerative medicine comes in the form of corundum ceramic composites modified with various additives (bioglass polymers) obtained by different techniques. Most researchers studying corundum implants and their use in modern bone surgery claim that corundum material does not produce strong chemical connection with bone tissue. The addition of corundum bioglass from the $CaO$-$P_2O_5$-$SiO_2$-$Na_2O$ system into the corundum matrix affects mostly the possibility of creating chemical bonding with bone tissue. Modifying the composite with bioglass results in obtaining new strength characteristics, which also affects surface properties that appear to cause increased cell proliferation. Corundum ceramic composites modified with bio-glasses are characterized by [5,6,7,8]:

- porosity that enables tissue ingrowth, securing permanent connection between tissue and implant,
- high biocompatibility and bioactivity in the tissue environment,
- high compressive strength and abrasion resistance,
- possibility of sterilization without changing the properties of materials,
- easy shaping of the material by conventional means,

Currently ceramic composites containing bioglass and glass-ceramics are already used not only as experimental material but also in clinical practice [5,9,10] as:

- middle ear implants (solid MEP® and Douek-MED™ fittings – Bioglass® 45S5 Cervital®),
- restoration after tooth extraction (solid REMI® – Bioglass 45S5 shapes),
- filling of bone defects (powder or granules: PerioGlas® Biogran® – Bioglass® 45S5; powder and granules: BinAlive-glass S53P4; granules: Cerabone®),
- implants and fillings in craniofacial surgery (NoveBone® lite powder, Ilmaplant® shapes),
- porous scaffolds for tissue engineering,
- drug delivery system.

## Subject Matter And Methodology

After preliminary analysis of ten biocomposites, two were finally selected for further research. The two kinds of biocomposites (W5, W7) containing submicrocrystalline sintered corundum and bioglass from $Ca0\text{-}Si0_2\text{-}P_20_5\text{-}Na_20$ system with various proportion of the components (W5-50%vol of glass, W7-70%vol of glass ) respectively.

Physical and mechanical properties (microscopic observation, porosity, absorbability, HRB hardness) were tested on 16x5 mm and 10x2 mm tablets obtained by cold pressing under 75 MPa pressure and freely sintered in an electric furnace. The heat treatment process was carried out according to predetermined characteristics with stabilisation for two hours at maximum temperature (770$^{o}$C).

Chemical stability calculations at the maximum temperature (750$^{o}$C, 770$^{o}$C) were carried out using the VCS algorithm. Verification of the obtained results was performed using Emprean Diffractometer with Cu radiation fully confirming the presence of the calculated compounds. Microscopic observations on the Joel JSM6460 LV scanning electron microscope were made in high vacuum ($10^5$ Torr) at an accelerating voltage of 20kV, magnification 40x and 100x using the BEC image. The geometric structure of the surface was determined using the TOPO01vP profilometer through the measurements of surface topography parameters ($R_a$, $R_z$, $R_t$) and 2D and 3D spatial images.

The hardness of bio composites was determined by reading the values of 1/6 inch steel ball res-cess on the HRB scale on the Rockvell hardness tester. Biocompatibility of the composites was determined by SBF test (immersion of composite samples in artificial blood plasma for 30 days). The surface of

composites after a long-term bath on a scanning microscope BEC image was observed and the phase composition of the surface of composites was also analysed. Human chondrocyte cells were seeded on the obtained tablets (as growth media) using standard procedure (CGH Lanza medium, 37$^{o}$C in 5% $CO_2$ atmosphere, initial cell density 1x10 $^4$ cells/cm$^2$) and WST-1 proliferation assay was performed (reading after 72h, 96h, 144h with positive results).

# 2.1 Some physical and mechanical properties of raw and sintered materials

The raw materials used in sintering process were: submicrocrystalline sintered corundum of F 320 (49 – 16,5 um) and glass from CaO-$P_2O_5$ $SiO_2$-$Na_2O$ system marked as FB1 with grain size of about 40 μm. Submicrocrystalline sintered corundum grain is new generation of alfa type aluminium oxide with ultradispersive structure. It might be obtained by transformation of sol-gel process of aluminium oxide by using MgO, $L_2O_3$ $Nd_2O_3$ $Y_2O_3$ as modifiers. Abrasive grains consist of $Al_2O_3$ plates about 0,5 – 1 μm joint by needle bridge of $MgLaAl_{11}O_{19}$ spinel type. In comparison to conventional corundum materials submicrocrystalline sintered corundum grains have higher strength (90 MPa, conventional 80 MPa), hardness (20-22GPa, conventional18,5-20GPa) with simultaneously increase of fracture toughness. Commercial names of these materials are cubitron, Seeded Gel and Blue Sapphire [13].

FB1 glass obtained from CaO-$SiO_2$-$P_2O_5$-$Na_2O$ was melted at 1350$^{o}$C in electric furnace in air atmosphere and then fritted (poured into cold water). Obtained material belongs to the group of light weight materials, as its density is of Material has 2.622 g/cm3. Materials belongs to medium hard glasses about4.9MPa. ) which have good wettability to cubitron substrate (contact angle $\theta < 30^{o}$ at 850$^{o}$C).

The sinters (W5 and W7 selected from ten among previously tested), were obtained by powder metallurgy technique through free sinters in electric furnace in air atmosphere. Their physical and mechanical properties differ significantly – Table 1.

Table 1
Chosen properties of tested materials W5 and W7 samples

| Compositions variants | Composite density [g/cm3] | Theoretical porosity [%] | Open porosity tested [%] | Absorbability tested [%] | Hardness [HRB] |
|---|---|---|---|---|---|
| W5 | 3.328 | 21,5 ± 0.1 | 20.35 ± 0. 3 | 8.4 ± 0,1 | 60 |
| W7 | 2.850 | 2.1 ± 0.02 | 1.25 ± 0.01 | 0.5 ± 0.04 | 78 |

Increasing the glass content caused a decrease in the density of the composite and a significant decrease in open porosity

# 2.2 Calculation of chemical equilibrium of biocomposites using VCS algorithm

The chemical stability of the sample of the submicrocrystalline sintered corundum – glass of $CaO$-$P_2O_5$-$SiO_2$-$Na_2O$ system was determined by calculating the thermodynamic potential ΔG of the reactions likely to occur between them. The calculations were performed using the VCS algorithm (Villers, Cruise and Smith), taking into account the chemical stability of all probable reaction products.

Equilibrium calculations were done with the method of minimizing the thermodynamic potential of the entire mixture. The mass balance of elements and non-negativity of the mole numbers of individual components was maintained. In this method, the equilibrium composition means a non-negative set of moles of individual components for which the thermodynamic potential ΔG of the entire mixture reaches a minimum while meeting the mass balance equations of all elements of the mixture. The formula used was:

$$\Delta G = \sum_{i=1}^{N} n_i \mu_i \qquad (1)$$

Where:

ΔG - thermodynamic potential

$n_i$ – number of moles of components i

$\mu_i$ – chemical potential of components i

N – number of ingredients

Equilibrium calculations with the minimizing thermodynamic potential method did not require any specifying number and form of reactions through which the system reached equilibrium. Specification of the substances that may or may not be in balance was necessary. The premise of the method is that all connections possible from the elements included in the mixture in the equilibrium state could have occurred. The calculations showed that 7 compounds from 100 available mixtures make it possible to create solid state connections. The calculations took into account the number of gram-atoms of glass components and sintered microcrystalline corundum in specific volumes.

For W7, the number of gram-atoms of bioglass components in the volume of 700 $cm^3$ and the number of gram-atoms of submicrocrystalline corundum sintered in 300 $cm^3$ of composite were calculated.

For W5, the number of gram-atoms of bioglass components in the volume of 500 $cm^3$ and the number of gram-atoms of submicrocrystalline corundum sintered in 500 $cm^3$ of composite were calculated.

The assumption was made that the components of biocomposites in these temperature ranges (750°C and 770°C) could have occurred: in the multi-component gas phase, pure condensed phases (liquid and solid), and the liquid phase in which the components were mixed unrestrictedly.

Assumption I: the resulting equilibrium mixture consisted of a multi-component gas phase and pure condensed phases (solid and liquid) that do not mix.

Assumption II: the resulting equilibrium mixture consists of a multi-component gas phase, a multi-component liquid phase, and pure solid phases.

The equilibrium composition in the number of moles is the same for both these assumptions.

Table 3
VCS algorithm calculation conditions.

| **T [K]** | **1023.15** | **1043.15** |
|---|---|---|
| t [°C] | 750 | 770 |
| P [atm] | 1.00 | 1.00 |

Tables 4 and 5 show the compositions of equilibrium systems of w5 and w7 biocomposites at 750°C, 770°C for condensed phases

Table 4
Stable solid compounds according to Assumptions I and II for W5 sample

| **Variant W5** | **Assumption I** | | **Assumption II** | |
|---|---|---|---|---|
| Phase composition | 750°C | 770°C | 750°C | 770°C |
| $Al_2O_3$ | 14.200 | 14.200 | 14.200 | 14.200 |
| $SiO_2$ | 3.100 | 3.100 | 3.100 | 3.100 |
| $CaAl_2Si_2O_8$ | 1.345 | 1.345 | 1.345 | 1.345 |
| $Ca_3(PO_4)_2$ | 0.250 | 0.250 | 0.170 | 0.170 |
| $Ca_2Al_4O_7$ | 1.119 | 1.119 | 1.119 | 1.119 |
| $NaAlSiO_4$ | 0.521 | 0.521 | 0.521 | 0.521 |

Table 5
Stable solid compounds according to Assumptions I and II for W7 sample

| Variant W7 | Assumption I | | Assumption II | |
|---|---|---|---|---|
| Phase composition | 750°C | 770°C | 750°C | 770°C |
| $Al_2O_3$ | 11.900 | 11.900 | 11.900 | 11.900 |
| $SiO_2$ | 4.020 | 4.020 | 4.020 | 4.020 |
| $CaAl_2Si_2O_8$ | 1.520 | 1.520 | 1.520 | 1.520 |
| $Ca_3(PO_4)_2$ | 0.400 | 0.400 | 0.320 | 0.320 |
| $Ca_2Al_4O_7$ | 1.321 | 1.321 | 1.321 | 1.321 |
| $NaAlSiO_4$ | 0.645 | 0.645 | 0.645 | 0.645 |

Verification of the obtained results was performed by use of XRD – phase analyses.

# 2.3 XRD analyses of W5, W7 bio composites

The X-ray experiment was performed with the PANalytical Empyrean Diffractometer with Cu radiation. Phase analysis basing on ICDD PDF 4 + 2017 data base confirmed the presence of $Al_2O_3$, $SiO_2$, $CaAl_2Si_2O_8$, $Ca_3(PO_4)_2$, $Ca_2Al_4O_7$, $NaAlSiO_4$ phases. The X-ray diffraction patterns are presented on the Figs. 2 and 3. The detailed structural characteristic of tested W5 and W7 samples are presented in Tables 5 and 6.

The determination of unit cell parameters, crystallite sizes and lattice strain values as well as qualitative phase analysis were refined by using the PANalytical software High Score Plus basing on the Rietveld method [15,16]. The scheme of analyses and conditions were presented, among others in [17,18].

Table 6
Structural analysis of W5 sample.

| Phase | Space Group | Amount [%] | a [Å] | b [Å] | c [Å] | D [Å] | ε [%] |
|---|---|---|---|---|---|---|---|
| $Al_2O_3$ | R-3c | 42 | 4.7587(7) | | 12.9926(5) | > 1000 | 0.075 |
| $SiO_2$ | $P3_22_1$ | 10 | 4.9212(2) | | 5.4104(1) | 456 | 0.072 |
| $CaAl_2Si_2O_8$ | P-1 | 9 | 8.1591(7) | 12.6111(6) | 12.9240(8) | 364 | 0.421 |
| $CaAl_4O_7$ | C2/c | 25 | 13.0595(1) | 9.1355(1) | 5.4668(6) | 73 | 0.447 |
| $NaAlSiO_4$ | $P6_3$ | 10 | 9.9806(8) | | 8.2909(7) | 232 | 0.140 |
| $Ca_3(PO_4)_2$ | $P2_1/c$ | 4 | 5.0088(5) | 18.2004(9) | | 275 | 0.119 |

Table 6
Structural analysis of W7 sample.

| Phase | Space Group | Amount [%] | a [Å] | b [Å] | c [Å] | D [Å] | ε [%] |
|---|---|---|---|---|---|---|---|
| $Al_2O_3$ | R-3c | 35 | 4.7574(4) | | 12.9936(2) | 730 | 0.045 |
| $SiO_2$ | $P3_22_1$ | 6 | 4.9527(7) | | 5.2503(2) | 129 | 0.253 |
| $CaAl_2Si_2O_8$ | P-1 | 14 | 8.1355(2) | 12.8189(9) | 12.6271(1) | 323 | 0.101 |
| $CaAl_4O_7$ | C2/c | 31 | 12.8378(2) | 9.1979(5) | 5.3604(8) | 123 | 0.266 |
| $NaAlSiO_4$ | $P6_3$ | 10 | 9.9386(2) | | 8.3157(8) | 286 | 0.114 |
| $Ca_3(PO_4)_2$ | $P2_1/c$ | 4 | 4.7632(9) | 18.8053(1) | | 491 | 0.067 |

In comparison to the theoretical unit cell values (ICDD PDF + 4 2017 data base) of identified phases, the unit cell parameters were slightly changed. The tested material showed the presence of nanocrystalline phases, with crystallite sizes from 100 to 450 Å. Only the size of corundum crystallites is in the order of 750–1000 Å.

# 2.4 Microscopic observations

Microscopic observations of the W5 and W7 bio composites on a scanning electron microscope (SEM, BEC image) showed, in the case of the W5 sample, uneven coating of glass sintered over submicrocrystalline corundum grains, particularly visible at the grain boundaries. Few deep pores appeared on the surface. The surface of the W7 bio composite sample was evenly covered with glass (Fig. 4) with only a few small pores, which was confirmed by studies of the surfaces

# 2.5 Topography of composite surfaces

The measurement of the geometric surface of the W5 and W7 samples showed clear differences in the surface topography by $R_p$ parameters (height of the highest profile rise inside the elementary segment W5 11.764 µm, W7 11.390 µm), $R_z$ (sum of height of the highest rise and largest indentation in the elementary section W5 34.04 µm, W7 44.04 µm, and $R_t$ (sum of height of the highest rise and largest indentation of the measured section W5 46.283 µm, W7 66.434 µm). This confirmed the impact of the glass content on the origination of fine deep pores on composite surface. Togethre with theincreasing content of bioglass in the composite, the increase in the number of small-width pores was observed. Symmetrical system was found in the analysis of the material share graph of the W5 sample, without characteristic, random extreme surface elements (rises and indentations). In case of the W7 sample, the material share graph showed an upward shift, which proved occurrence of individual narrow, deep cavities.

# 2.6 SBF test

Samples of W5 and W7 composite scaffolds were prepared for the SBF test by heating in an electric oven at 300°C for 1 hour, washing with 96% ethanol, and steam sterilising in an autoclave at 120°C. The samples were immersed in an artificial blood plasma (SBF) solution that was previously filtered with a 0.22 µm syringe filter. pH of the SBF solution after removing the samples after 30 days was 7.61. The SEM/EDX analysis after the final incubation period showed no significant surface changes for W5 sample, with only larger pores occurring. It was most likely that the $Na^+$ ions from glass were exchanged for H + ions from SBF solution resalted in a layer rich in Si (a layer of silica gel) However, no crystallization of calcium phosphates was observed, which might probable be associeted with a positive surface charge due to a high content of $Al_2O_3$

The entire surface of the W7 sample presented fine spherical forms with morphology characteristic of HA-hydroxyapatite. EDX analysis showed that only P and Ca were present on the surface. The Ca/P ratio was 1.55, which proved the formation of HA with Ca deficit. The presence of $Na^+$ and $Mg^{2+}$ ions in the surface layer composition most likely means the share of these elements in the structure of forming HA as a substitution in the cationic subnet.

# 2.7 Pre-culture of human chondrocyte cells on biocomposite scaffolds.

Preparation of biocomposite scaffolds for seeding of human chondrocyte cells consisted of sterilisation by 24 h incubation with 70% Et0H and UV lamp irradiation for 40 min on each side. The proliferation assay was performed using the Cell proliferation reagent WST-1 kit (Roche Diagnostics) based on the measurement of cell reduction potential. As the number of cultured cells increases, the amount of reducing enzymes increases, which is measured at appropriate time points (72, 96, 144h) by determining the absorbance of the samples. These are the filtrate from incubation of cells with culture medium with reagent added. NHAC-kn cells were seeded for the test (Lonza cell source) at an initial density of 1x10 4cell/$cm^2$. The reference medium was polystyrene medium. A plot of the time dependence of the

absorbance values for the composites tested (W5, W7) is shown below. It was found that the chondrocytes adhered to the media and the tested media allowed cell proliferation. However, the proliferation rate was lower than under control conditions and no significant differences were observed in proliferation to W5 and W7 scaffolds.

Experiments were performed twice in triplicate for each experimental condition. Data represent mean values ± SD. Statistical analysis was performed using GraphPad Prism8.0.

# Conclusion

The following concludes the studies of W5 and W7 composite scaffolds with submicrocrystalline sintered corundum and FB1 bioglass:

- Increasing the FB1 glass content (from 50–70% by volume) significantly affected open porosity of sinters and their absorptivity (W5: porosity 20%, absorptivity 8.4%; W7: porosity 1.25%, absorptivity 0.5%);
- VCS calculations verified by X-ray tests showed the presence of $Al_2O_3$, $SiO_2$, $CaAl_2Si_2O_8$, $CaAl_4O_7$, $NaAlSiO_4$ and $Ca_3(PO_4)_2$ in both composites;
- Microscopic image (SEM, BEC) of W5 scaffold composites showed incomplete FB1 glass coverage of sintered microcrystalline corundum grains and visible large pores between corundum grains (Fig. 1). The W7 composite surface, however, was evenly covered with glass with narrow, fine pores;
- Measurements of the geometric surface of scaffolds W5 and W7 showed clear differences in the parameters: $R_p$ (W5–11.764 µm, W7–11.390 µm), $R_z$ (W5–34.04 µm, W7–44.04 µm), and $R_t$ (W5–46.283 µm, W7–66.434 µm). The graph of W7 sinter material showed upward shift, which indicated the presence of narrow, deep cavities;
- SEM/EDX analysis of scaffolds after 30 days of SBF (artificial blood plasma) bathing showed no significant surface changes in W5 sample. Partial glass corrosion probably occurred. The W7 sinter surface, however, was covered with spherical forms characteristic of HA-hydroxyapatite. EDX analysis confirmed the presence of only Ca and P in a ratio of Ca/P 1.55, which indicated the formation of HA with Ca deficiency.
- Both substrates (W5 and W7) were biocompatible despite differences in SBF assay behaviour, as confirmed by the WST-1 assay. The substrates tested allowed for the proliferation of human chondrocyte cells (increase in absorbance in the WST-1 assay with increasing incubation time), however, the proliferation rate was lower than in the reference medium. No significant differences in cell proliferation were observed between the media

# Declarations

**Acknowledgment:** The project was carried out with the Łukasiewicz - Krakow Institute of Technology own founds

**Author Contributions:** Conceptualization, B.S.-B.; Methodology, B.S.-B., J. D. and M.K.; Validation, B.S.-B., M.K.; Formal

Analysis: B.S.-B., J.D., J.L.-Ł.,K.C.-K., J.S., K.S., G.S. and M.K.; Investigation, B.S.-B., J.D., J.L.-Ł.,K.C.-K., J.S., K.S., G.S. and M.K.; Resources, B.S.-B.; M.K., Data Curation, B.S.-B.; Writing—Original Draft Preparation, B.S.-B.; Writing—Review and Editing, B.S.-B.,; Visualization, B.S.-B., G.S., and M.K., Supervision, B.S.-B.; Project Administration, B.S.-B.; Funding Acquisition, B.S.-B.

**Funding:** The project was carried out at Łukasiewicz – IAMT own funds.

**Conflicts of Interest:** The authors declare no conflict of interest.

**Compliance with Ethical Standards:** There is no research involving Human Participants and Animals.

**Availability of data and material (data transparency):** Not applicable.

**Code availability (software application or custom code):** Not applicable.

# References

[1] Błażewicz S., Stoch L.: *Biomaterials, vol. 4.Akademicka Oficyna Wydawnicza Exit,* Warszawa 2003

[2] Świeczko-Żurek B.: *Biomaterials, WPG* 2009

[3] Boccaccini A.R., Gerhardt L.C.: Bioactive glass and glass-ceramic scaffolds for bone tissue engineering, [ed:] *Materials* 2010, 3, 2867–3910

[4] Ratner B.D., Hoffman A.S., Schoen F.J., Lemons J.E.: Biomaterials Science: An introduction to materials in medicine, ed. *Academic Press,* 1996

[5] Dziadek M., Pawlik J., Cholewa-Kowalska K.: Bioactive glasses for tissue engineering Acta Bio-Optica et Informatica Medica - Inżynieria Biomedyczna 2014 vol 20 no 3, pp 156–165

[6] Dziadek M., Zagrajczuk B., Jeleń P., Olejniczak Z., Cholewa-Kowalska K.: Structural variations of bioactive glasses obtained by different synthesis routes, Ceramics International Volume 42, Issue 13, 2016, pp 14700–14709, https://doi.org/10.1016/j.ceramint.2016.06.095

[7] Sachlos E., Czernuszka J. T.: Making tissue engineering scaffolds work. Review on the application of solid freeform fabrication technology to the production of tissue engineering scaffolds. European Cells and Materials, AO Research Institute Davos, Davos 2003

[8] Staniewicz-Brudnik B., Lekka M.: Biocompatible glass-ceramic composite- manufacturing and selected physicalmechanical properties. Sintering of Ceramics, new Emerging Techniques / Book. ISBN 978-953-51-0017-1. Ed: Prof. Dr Arunachalam Lakshmanan. Saveetha Engineering College, Thandalam, Chennai, India, chapter 11 pp. 227–250, 2012

[9] Yang F., Li C., Lin Y., Wang C. A.: Effects of sintering temperature on properties of porous mullite/corundum ceramics [in:] Materials Letters 73 (2012) pp. 36–39; https://doi.org/10.1016/j.matlet.2011.12.087

[10] Jaegermann Z., Ślósarczyk A.: Dense and porous corundum bioceramics in medical application. Uczelniane Wydawnictwo Naukowo–Dydaktyczne AGH, Kraków 2007, (in Polish)

[11] Staniewicz-Brudnik B., Lekka M., Bączek E., Wodnicka K., Miller T., Wilk W.: Biocomposites with submicrocrystalline sintered corundum and bioglass system as a scaffolds and their structural and physical properties. Short- and long-term culture of the fibroblast human skin on these substrate. Optica Applicata. Vol XLII, 2, pp 387–397, Wrocław 2012, DOI: 10.5277/oa120216

[12] Staniewicz-Brudnik B., Lekka M., Jaworska L., Wilk W.: Biocompatible glass composite system – some physical-mechanical properties of the glass composite matrix system. Optica Applicata, Institute of Physics, Wrocław University of Technology, Wrocław 2010

[13] Niżankowski Cz.: Manufacturing sintered corundum abradants. Archives of Civil and Mechanical Engineering, Faculty of Mechanical Engineering Wrocław University of Technology, Wrocław 2002

[14] Staniewicz-Brudnik B., Szarska S. and Gamrat K.: The influence of mechanochemical treatment of sintered submicrocrystalline corundum scaffolds on the structure of bioglass composites. Journal of Superhard Materials, Volume 30, Number 6 (2008), 392–399, DOI: 10. 3103/S1063457608060051

[15] Young RA. The Rietveld method. Oxford University Press; 1993.

[16] McCusker LB, Von Dreele RB, Cox DE, et al. Rietveld refinement guidelines. J. Appl. Crystallogr. 32, 1999, 36–50. https://doi.org/10.1107/S0021889898009856

[17] Karolus M., Łągiewka E.: Crystallite size and lattice strain in nanocrystalline Ni-Mo alloys studied by Rietveld Refinement. Journal of Alloys and Compounds 367 (2004) 235-238. DOI: 10.1016/j.jallcom.2003.08.044

[18] Karolus M.: Applications of Rietveld refinement in Fe-B-Nb alloy structure studies. Journal of Materials Processing Technology 175 (2006) 246 - 250. https://doi.org/10.1016/j.jmatprotec.2005.04.016

# Tables

Table 2 is not available with this version

# Figures

Image not available with this version

**Figure 1**

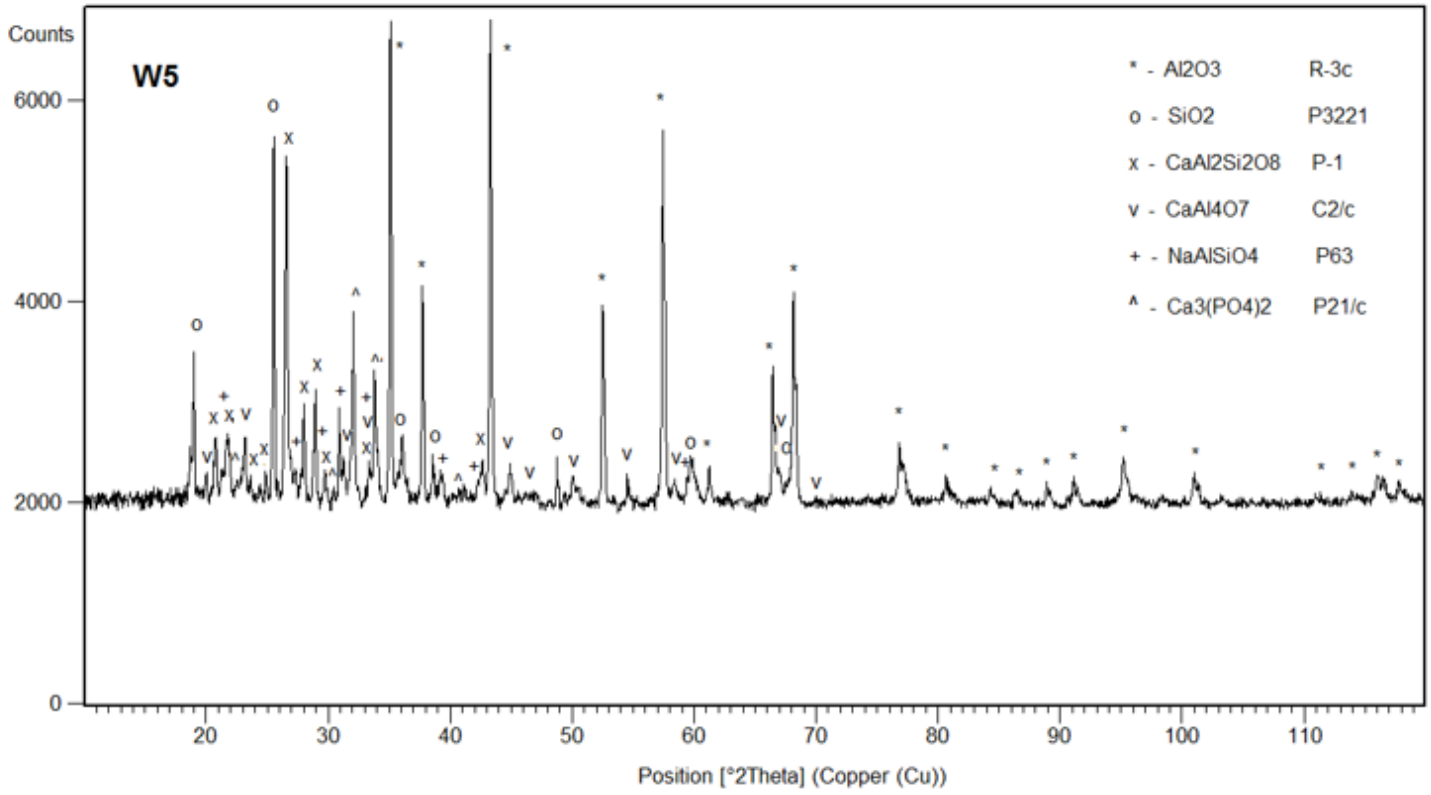


**Figure 2**

X-ray diffraction pattern of W5 sample.

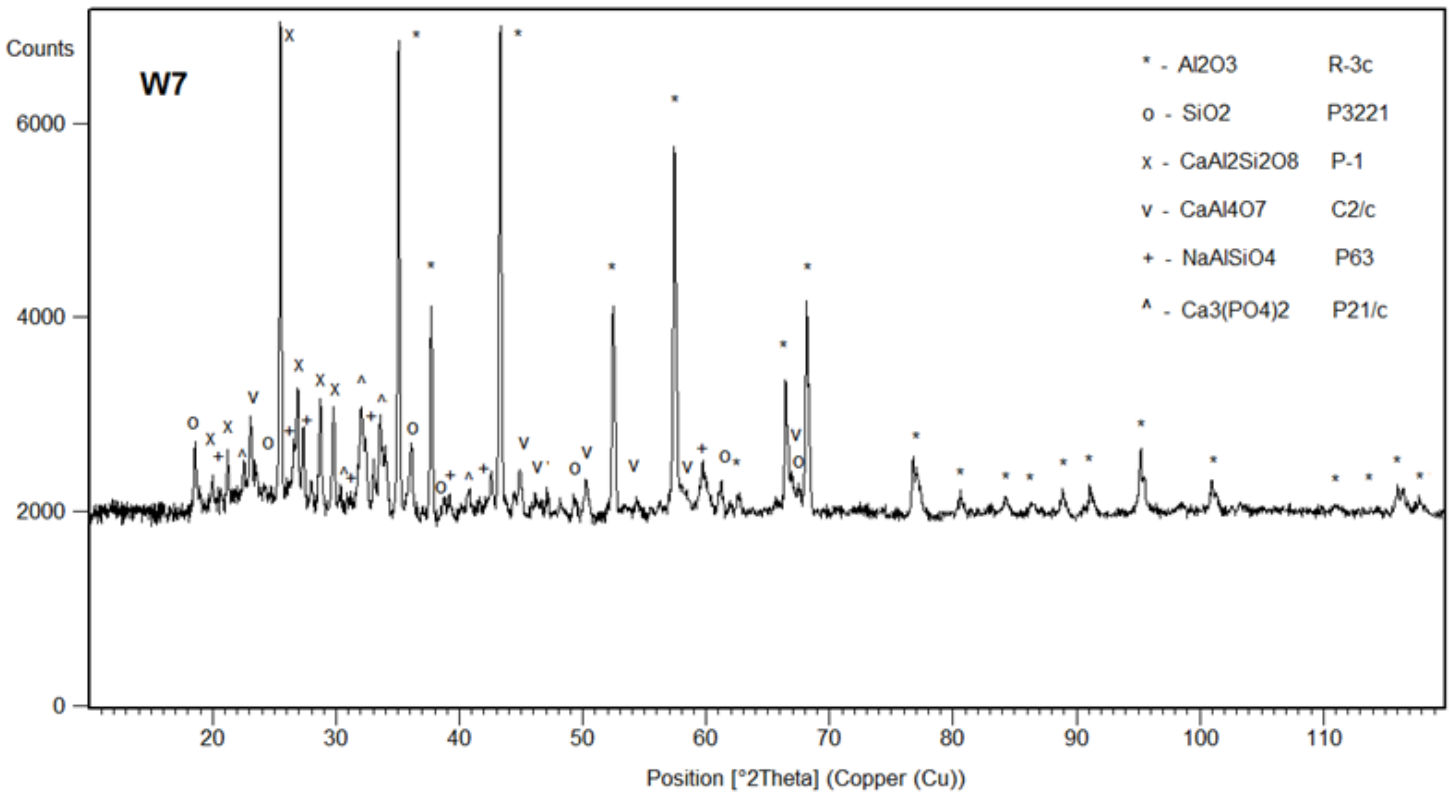


## Figure 3

X-ray diffraction pattern of W7 sample.

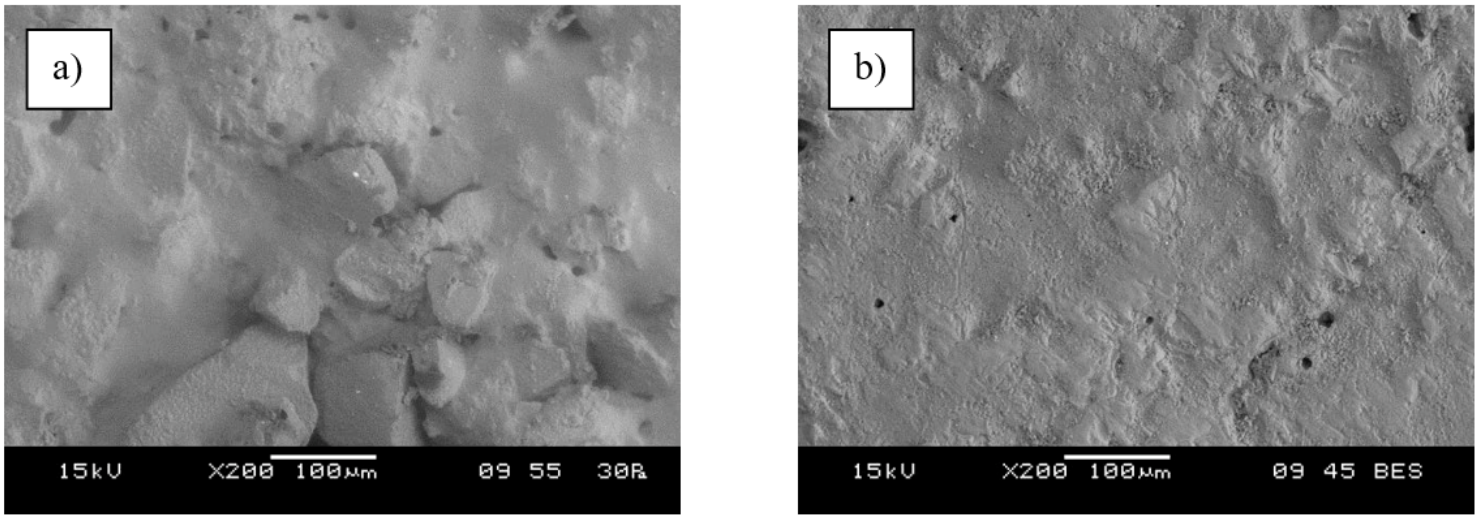


## Figure 4

SEM micrograph of the surface of W5 (a) and W7 (b) samples at 200x magnification.

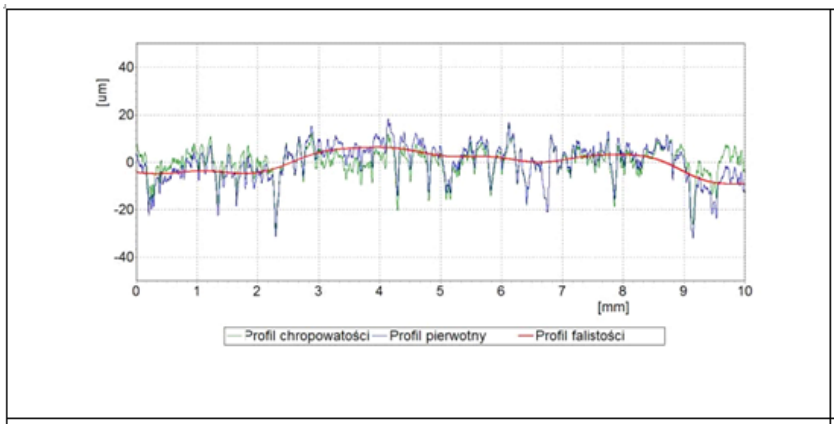


a)

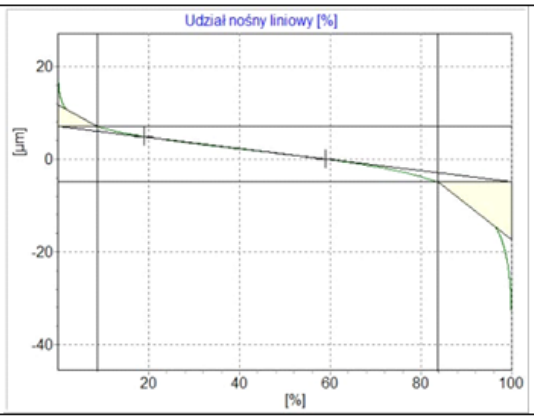


b)

| | Avg | S | Min | Max | Spacing |
|---|---|---|---|---|---|
| Ra [µm] | 4.644 | 0.511 | 3.510 | 6.101 | 2.592 |
| Rq [µm] | 6.237 | 0.707 | 4.724 | 8.467 | 3.743 |
| Rp [µm] | 11.764 | 1.319 | 9.033 | 16.714 | 7.680 |
| Rv [µm] | 22.642 | 3.039 | 15.507 | 31.115 | 15.608 |
| Rz [µm] | 34.406 | 3.592 | 26.089 | 44.220 | 18.131 |
| Rc [µm] | 11.346 | 1.519 | 8.033 | 15.561 | 7.528 |
| Rt [µm] | 46.283 | 5.903 | 31.574 | 63.822 | 32.248 |

c)

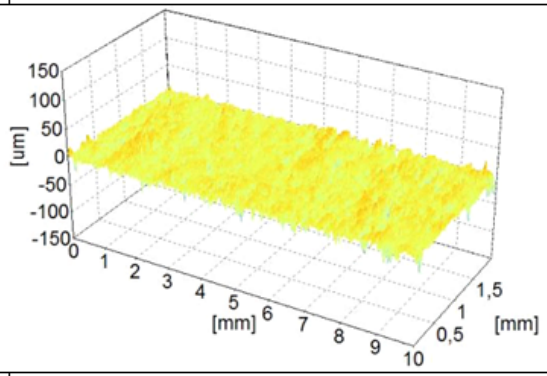


d)

## Figure 5

Topography of the W5 sample surface: roughness profile (a), linear load share (b), horizontal parameter values (c), surface map (d).

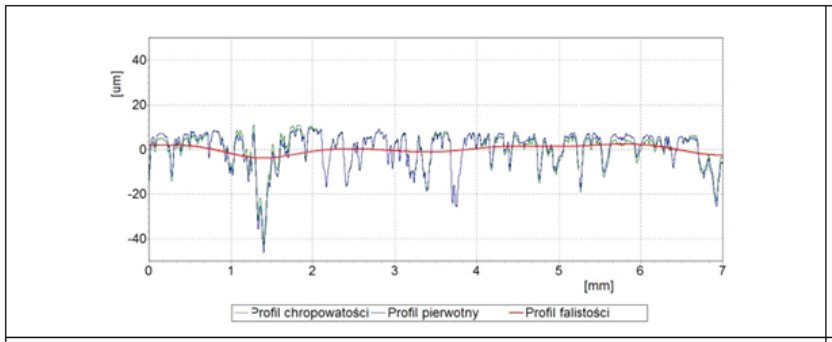


a)

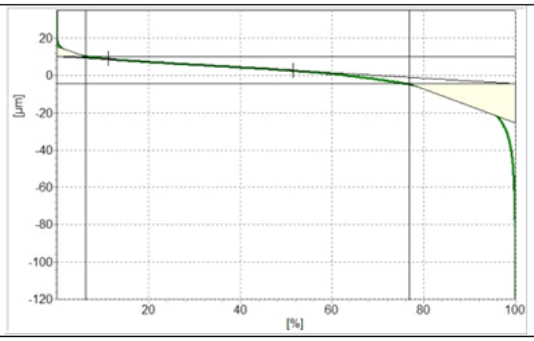


b)

| | Avg | S | Min | Max | Spacing |
|---|---|---|---|---|---|
| Ra [µm] | 7.459 | 1.423 | 4.463 | 11.807 | 7.344 |
| Rq [µm] | 9.845 | 2.274 | 5.899 | 17.651 | 11.752 |
| Rp [µm] | 11.390 | 2.159 | 6.829 | 19.787 | 12.958 |
| Rv [µm] | 33.295 | 8.849 | 19.800 | 64.965 | 45.165 |
| Rz [µm] | 44.685 | 10.542 | 26.805 | 80.696 | 53.891 |
| Rc [µm] | 18.611 | 4.324 | 11.937 | 47.025 | 35.088 |
| Rt [µm] | 68.434 | 22.656 | 34.939 | 141.764 | 106.825 |

c)

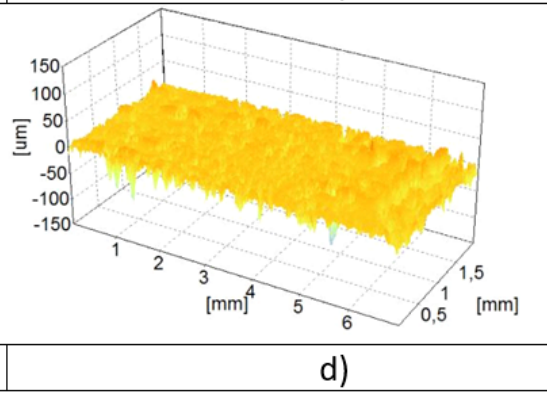


d)

## Figure 6

Topography of the W7 sample surface: roughness profile (a), linear load share (b), horizontal pa-rameter values (c), surface map (d).

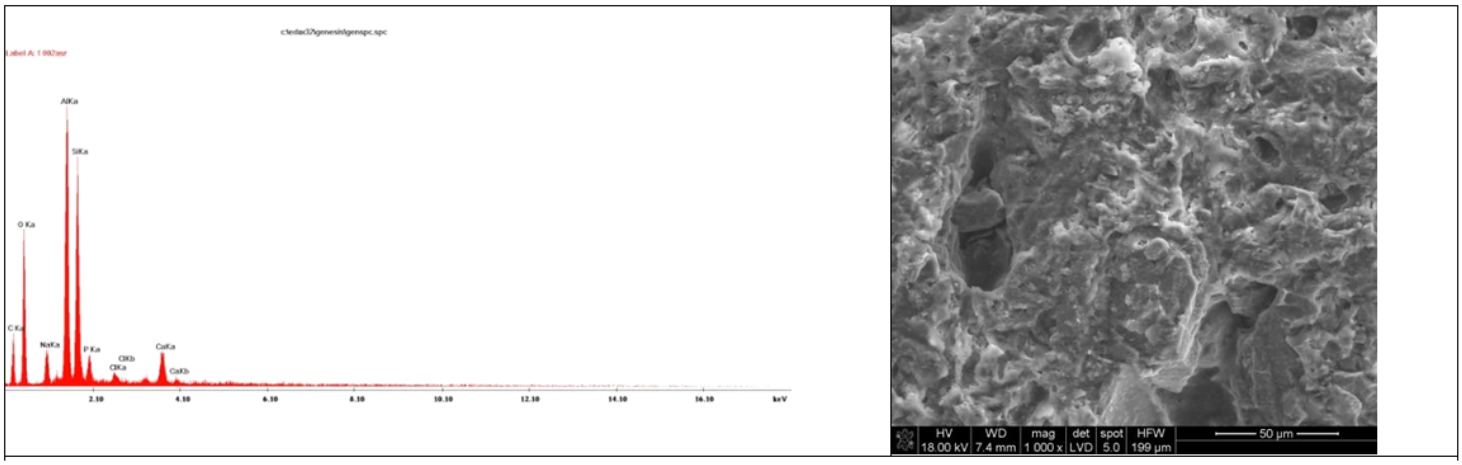


a

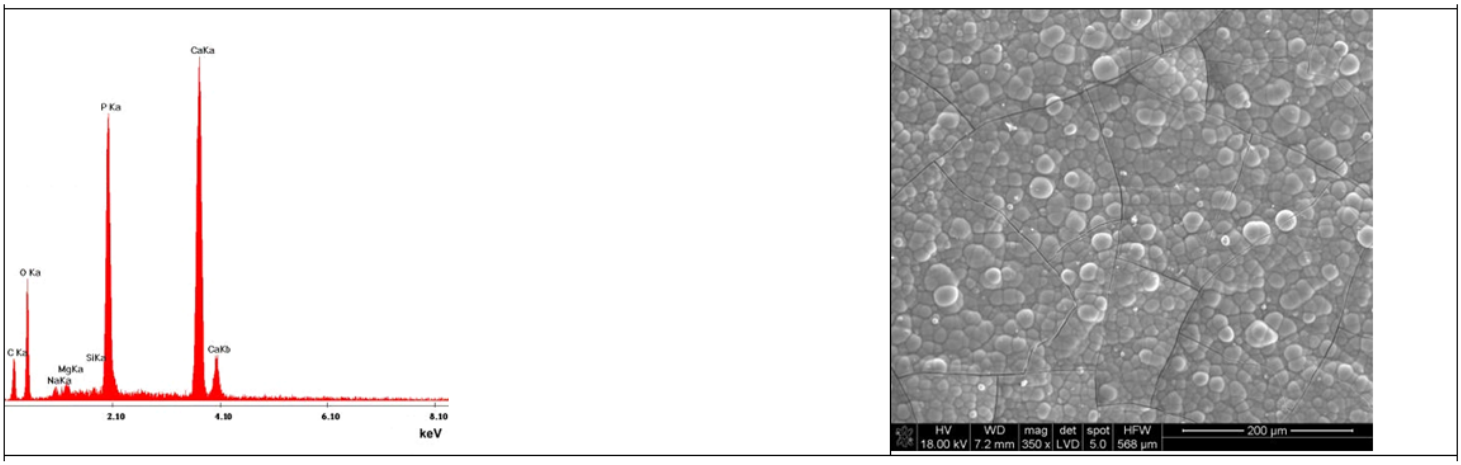


b

## Figure 7

a Microphotographs of SEM and EDS diagram of W5 sample b Microphotographs of SEM and EDS diagram of W7sample

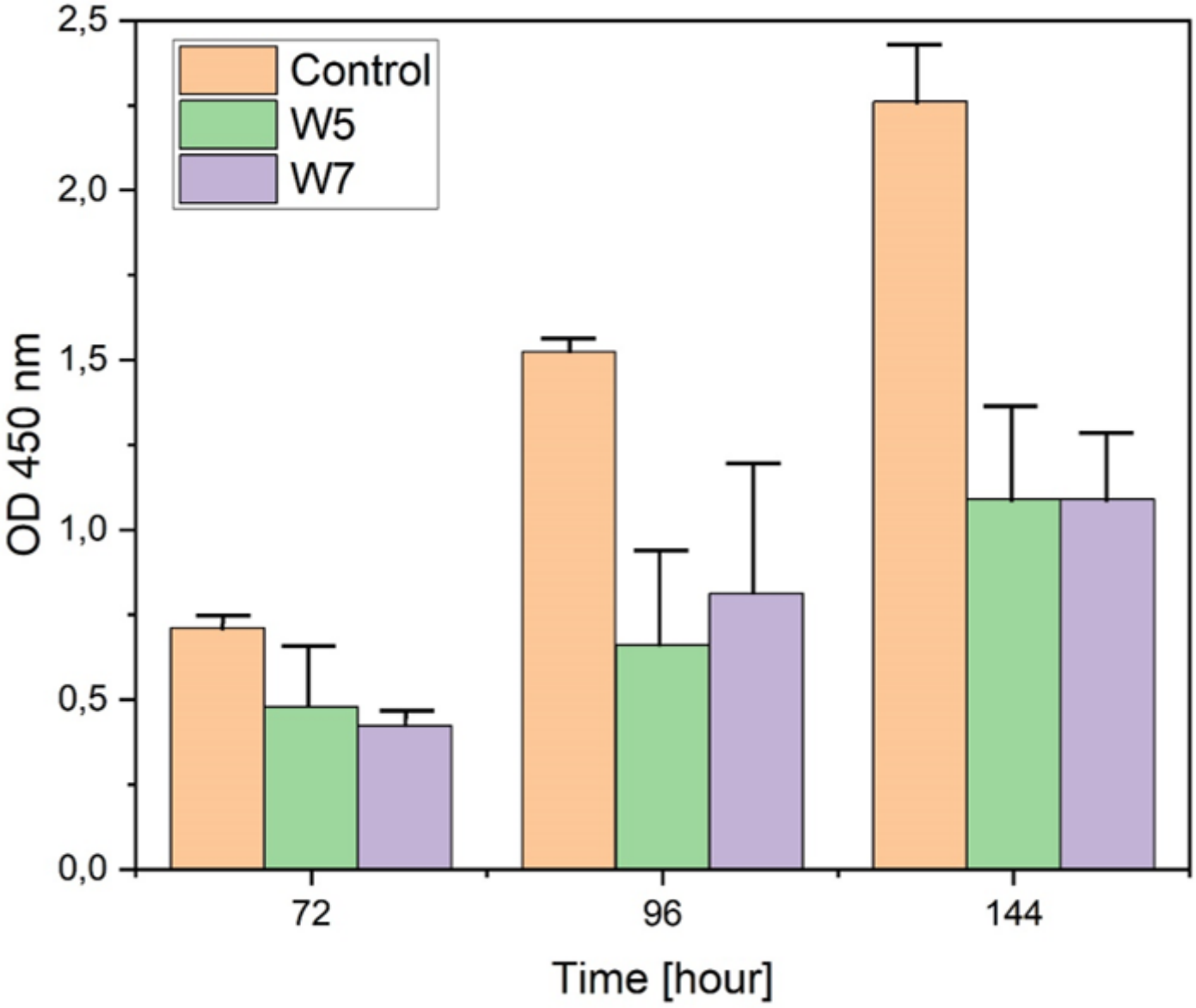


**Figure 8**

WST-1 cell proliferation test.